Redox Biology 37 (2020) 101623

Contents lists available at ScienceDirect

Redox Biology

journal homepage: www.elsevier.com/locate/redox

Research Paper

Oxidative stress in the retina and retinal pigment epithelium (RPE): Role of aging, and DJ-1

Mala Upadhyay [a], Caroline Milliner [a], Brent A. Bell [a,1], Vera L. Bonilha [a,b,*]

[a] Department of Ophthalmic Research, Cole Eye Institute, Cleveland Clinic, 9500 Euclid Avenue, Cleveland, OH, 44195, USA
[b] Department of Ophthalmology, Cleveland Clinic Lerner College of Medicine at Case Western Reserve University, Cleveland, OH, 44195, USA

ARTICLE INFO

Keywords:
Retina
Retinal pigment epithelium
Oxidative stress
Aging
DJ-1
Sodium iodate

ABSTRACT

High levels of oxidative radicals generated by daily light exposure and high metabolic rate suggest that the antioxidant machinery of the retina and retinal pigment epithelium (RPE) is crucial for their survival. DJ-1 is a redox-sensitive protein that has been shown to have neuroprotective function in the brain in Parkinson's disease and other neurodegenerative diseases. Here, we analyzed the role of DJ-1 in the retina during oxidative stress and aging. We induced low-level oxidative stress in young (3-month-old) and old (15-month-old) C57BL/6J (WT) and DJ-1 knockout (KO) mice and evaluated effects in the RPE and retina. Absence of DJ-1 resulted in increased retinal dysfunction in response to low levels of oxidative stress. Our findings suggest that loss of DJ-1 affects the RPE antioxidant machinery, rendering it unable to combat and neutralize low-level oxidative stress, irrespective of age. Moreover, they draw a parallel to the retinal degeneration observed in AMD, where the occurrence of genetic variants may leave the retina and RPE unable to fight sustained, low-levels of oxidative stress.

1. Introduction

Oxidative stress occurs when there is an imbalance between the generation of free radicals and the endogenous antioxidant defense mechanisms responsible for their elimination. These free radicals react and modify DNA, proteins, lipids, and saccharides. The precise cellular mechanisms underlying aging are still unclear, but it includes accumulation of oxidative damage and loss of function of organs, tissues, and cells [1]. We also know that experimental regimens such as caloric restriction in rodents extends life span and retards the buildup of molecular oxidative damage [2,3].

The retina and retinal pigment epithelium (RPE) are exposed to chronic oxidative stress. Light exposure induces high oxygen consumption, oxidization of polyunsaturated fatty acids, and phagocytosis of photoreceptor outer segments that result in the generation of high levels of free radicals daily [4]. Increased oxidative stress and progressive degeneration are associated with age-related macular degeneration (AMD), diabetic retinopathy, and glaucoma. Specifically, AMD is a disease of the outer retina that affects the RPE, choriocapillaris, and photoreceptors of the human macula, resulting in central field vision loss. The etiology of AMD is poorly understood; however, current hypotheses suggest that various genes interact with environmental factors to generate increased oxidative stress and inflammation [5].

DJ-1 is a multifunctional protein known to play a cytoprotective role and counteract oxidative stress in neurons [6,7]. Previously, we reported robust DJ-1 localization in the RPE and photoreceptor cells, mostly at the inner segments and cell bodies [8]. We also reported that loss of DJ-1 results in RPE thinning and mild physiological changes in the electroretinograms of 6-month-old DJ-1 knockout (KO) mice [8]. DJ-1 is one of several proteins whose concentrations are regulated during retinal postnatal maturation and with aging [9,10]. Indeed, we previously reported that without DJ-1, aged mice (18 months) display signs of retina and RPE degeneration accompanied by elevated levels of the oxidative markers protein carbonyl and inducible nitric oxide synthase. These observations suggest that DJ-1 has an essential, protective role in the retina during aging [11]. As the detailed mechanisms distinguishing retinal aging and degeneration are not fully elucidated, we analyzed the age-related changes to the structure and molecular composition of the retina during aging and in conditions of elevated stress. Here, we analyzed age-related changes to the structure and

Abbreviations: AGE, advanced glycation end product; AMD, age-related macular degeneration; BM, Bruch's membrane; CTCF, corrected total cell fluorescence; GFAP, anti-glial fibrillary acidic protein; PD, Parkinson's disease; ROS, reactive oxygen species; RPE, retinal pigment epithelium.

* Corresponding author. Department of Ophthalmic Research, Cole Eye Institute, Cleveland Clinic, 9500 Euclid Avenue, Cleveland, OH, 44195, USA.
E-mail address: bonilhav@ccf.org (V.L. Bonilha).
[1] Present address: Scheie Eye Institute, University of Pennsylvania, Philadelphia, PA 19104, USA.

https://doi.org/10.1016/j.redox.2020.101623
Received 20 March 2020; Received in revised form 22 June 2020; Accepted 24 June 2020
Available online 17 July 2020

molecular composition of the retina and RPE of C57BL and DJ-1 KO mice. These same parameters were analyzed in parallel experiments of mice subjected to low oxidative stress. Altogether, our data demonstrate that the absence of DJ-1 accelerates aging to some extent in the DJ-1 KO mice retinas and increases their -susceptibility- to oxidative damage and degeneration even under conditions of low oxidative stress and independently of age.

2. Materials and methods

2.1. Mice

All procedures were approved by the Institutional Animal Care and Use Committee (ARC 2016-1516) of the Cleveland Clinic. Experiments on both male and female DJ-1 KO and C57BL/6J mice have been previously described [8,11]. Mice were housed in individually ventilated cages in a 14-h light/10-h dark cycle and were provided regular chow and water ad libitum.

To induce selective RPE degeneration and atrophy, mice received a single tail vein injection of sodium iodate ($NaIO_3$; 10–20 mg/kg of body weight); the control group received PBS as previously described [8]. After mice were sacrificed on day 7 post injection (PI), the eyes were enucleated and processed for molecular, biochemical, and histological analyses.

2.2. Histology, imaging and bright-field microscopy

Enucleated eyes were fixed overnight at 4 °C in 2% paraformaldehyde, 2.5% glutaraldehyde, and 5% $CaCl_2$ in 0.1 M cacodylate buffer. After removal of the anterior segments using a dissecting microscope, eyecups were processed for epon embedding as previously described [8]. Semi-thin sections were cut using a diamond histotech knife (DiATOME, Hatfield, PA), collected on glass slides, and stained with toluidine blue. Sections were imaged with a Zeiss Axioimager. Z1 and MRc5 camera (Carl Zeiss AG, Oberkochen, Germany). Toluidine blue-stained images of eyecups (extending to the ora serrata) were acquired under identical settings. High magnification images were acquired within 200 μm of the optic nerve head (on both sides). Images were exported to ImageJ 2.0 software (NIH, Bethesda, MD) and calibrated using an embedded reference scale. Total and degenerated (absent and abnormal RPE) retinal areas were delineated using the free hand line tool. Degenerated areas were calculated for each sample according to following formula, degenerated area = (degenerated area/-total whole-mounts area) x 100 (as shown in Supplemental Fig. S1B).

2.3. Whole-mount RPE preparation, labeling, and degeneration quantification

Enucleated eyes were fixed for 20 min at 4 °C in 4% paraformaldehyde, after which retinas were mechanically detached from the RPE/choroid under a dissecting microscope and the RPE/choroid whole mounts processed for labeling with phalloidin-TRITC (1:1000; Sigma-Aldrich, St. Louis, MO) as previously described [11]. Whole-mount RPE/choroid samples were prepared on glass slides and images acquired using a laser scanning confocal microscope (TCS-SP8, Leica, Wetzlar, Germany). Serial Z-stacks and tiles of the whole-labeled RPE were collected, scans merged, and a three-dimensional projection of the entire whole-mount was generated. Images from four different mice in each group were acquired using identical settings. Quantification of RPE degeneration was calculated using ImageJ 2. Micrographs were calibrated from a reference scale embedded in the image. The outline of the whole RPE/choroid area and of the degenerated area (where RPE cells are present but their morphology is not the typical hexagonal shape) were delineated using the freehand line tool in ImageJ 2. Degenerated areas were calculated for each sample as described above and as shown in Supplemental Fig. S1A.

2.4. Retina immunohistochemistry

Enucleated eyes were, fixed by overnight immersion in 4% paraformaldehyde in D-PBS at 4 °C, and sequentially infused with sucrose and Tissue-Tek O.C.T Compound (4583; Sakura Finetek, Tokyo, Japan). Cryosections (8 μm) were cut on a cryostat HM 505E (Microm, Walldorf, Germany) equipped with a CryoJane Tape-Transfer system (Leica). For labeling, sections were washed, blocked in PBS supplemented with 1% BSA (PBS/BSA) for 30 min, and incubated with primary antibodies followed by secondary antibodies coupled to Alexa 488 or 594. Nuclei were labeled with TO-PRO-3 (Molecular Probes, Inc., Eugene, OR) as previously described [11]. Sections were analyzed using the Leica TCS-SP8. Antibodies used included Alexa Fluor 488 anti-glial fibrillary acidic protein (GFAP; 1:100; 53-9892-82; ThermoFisher Scientific, Waltham, MA), anti-glutamine synthetase (GS; 1:500; mouse antibody 610518; ThermoFisher Scientific), anti-AGE (1:200; rabbit ab23722; Abcam; Cambridge, MA), and anti-Nrf2 (1:100; rabbit ab31163; Abcam). Cryosections were also incubated with 10 μg/ml of Nile red (N1142; ThermoFisher Scientific) in PBS for 10 min at room temperature. Micrographs were calibrated from a scale reference embedded in the image. Quantification of Nile red staining frequency in the RPE cytoplasm was performed using the ImageJ "Point Picker" or "Cell Counter" plugins, and the number of lipid particles was calculated for each area according to the following formula, lipid particles/μm^2 = number of lipid droplets/area analyzed. Quantification of advanced glycation end product (AGE) immunoreactive signal intensity was also performed using ImageJ 2. Signal intensity was quantified within 200 μm of the optic nerve head, and the corrected total cell fluorescence (CTCF) was calculated for each area according to the following formula, CTCF = integrated density – (area of selected cell x mean fluorescence of background readings).

2.5. Retina and RPE isolation, RNA extraction, and qPCR

Under a dissecting microscope, the retina was mechanically detached from the RPE. RPE isolation was adapted from a method previously described [12]. Total RNA was isolated using the RNeasy Mini Kit (Qiagen, Hilden, Germany) according to manufacturer's instructions. cDNAs were synthesized from total RNA templates (250 ng of RPE RNA and 500 ng of retina RNA) using the Verso cDNA Kit (Thermo Fisher Scientific). qPCR was performed on a 7900HT Fast Real-Time PCR System (Life Technologies, Carlsbad, CA, USA) using the Radiant™ Green HI-ROX qPCR Kit (Alkali Scientific LLC, Fort Lauderdale, FL). Relative fold change was determined using $2^{-\Delta\Delta\ Ct}$ method and with Gapdh as the internal control. Obtained Ct values were normalized to C57Bl/6J mice. Primer sequences used in this study are listed in Supplemental Table 1. A list of the multiple comparison p-values for all the samples is provided in Supplemental Table 2.

2.6. Protein extraction and western blotting

Mechanically isolated retinas and RPE were lysed in RIPA buffer (Alfa Aesar, Havermill, MA) containing protein and phosphate inhibitors (Sigma-Aldrich). Retinas were sonicated twice for 15 s while RPE was passed through a 27 1/2 G syringe needle, incubated on ice, and vortexed every 5 min for 20 min. Both lysates were centrifuged for 10 min at 14000 rpm at 4 °C, after which the supernatants were collected for western blotting. Protein quantification was performed using the MicroBCA Kit (ThermoFisher Scientific), followed by: protein (30 μg) separation via 10–20% Novex Tricine SDS- PAGE (ThermoFisher Scientific) and transfer to PVDF membranes (Immobilon- FL; Merck Millipore; Burlington). Membranes were incubated with anti-Sod1 (1:1000; sc101523; Santa Cruz Biotechnology, Dallas, TX), anti-Prdx1 (1:1000; ab41906; Abcam), anti-DJ-1 (1:2000; NB300-270; Novus Biologicals, Littleton, CO), and anti-β-actin (1:4000; 8H10D10; Cell Signaling Technology, Danvers, MA) antibodies, followed by washing and

incubation with anti-mouse IRDye®680RD, anti-rabbit IRDye®680RD, and anti-mouse IRDye®800CW (all from LI-COR Biosciences, Lincoln, NE). Immunoreactive signals were visualized using Oddessey CLx (LI-COR Biosciences). The protein levels quantified using ImageStudio V5.2 software (LI-COR Biosciences). β-actin was used as internal control and C57BL/6J mice were used to normalize the calculated fold changes.

2.7. Proteomics analysis of retinas and RPE from young mice

Mechanically isolated retinas and RPE were lysed in RIPA buffer as described above. Proteins (30 μg) were resolved in 4–20% Novex®-Tris-Glycine gels (ThermoFisher Scientific), gels were fixed in 40% methanol, 10% Acetic acid and stained in Gelcode blue (ThermoFisher Scientific). Each gel lane was analyzed by dividing the gel lane into eleven areas and each area was prepared for proteomic analysis using an in-gel digestion protocol [13]. Briefly, the gel slices were washed, reduced with DTT, alkylated with iodoacetamide, and digested in situ with trypsin. Tryptic peptides were extracted as two aliquots with formic acid and acetonitrile, extracts were combined, dried with Speedvac and resuspended in acetic acid for LC-MS analysis. Peptides were analyzed in an Orbitrap Elite mass spectrometer system (ThermoScientific) equipped with an HPLC column (Dionex 15 cm x 75 μm id Acclaim Pepmap C18, 2 μm, 100 Å reversed-phase capillary chromatography column). Five μL volumes of the extract were injected and the peptides eluted from the column by an acetonitrile/0.1% formic acid gradient at a flow rate of 0.3 μL/min were introduced into the source of the mass spectrometer on-line using a LC gradient from 2 to 70% acetonitrile/0.1% formic acid in 110 min. The microelectrospray ion source is operated at 2.5 kV. The digest was analyzed using the data dependent multitask capability of the instrument acquiring full scan mass spectra to determine peptide molecular weights and product ion spectra to determine amino acid sequence in successive instrument scans. The LC-MS/MS data were analyzed using MaxQuant V1.5.2.8 with the search engine Andromeda which is integrated in the MaxQuant software and MS/MS spectra searched using the Uniprot mouse protein database [14]. The false discovery rate (FDR) was set to 1% at both the peptide and protein levels and two unique or razor peptides were required for positive identification. The "match between runs" feature of MaxQuant was used to transfer identifications to other LC-MS/MS runs based on their masses and retention time and quantifications performed with the label-free quantitation method in the MaxQuant program [15]. For the differential expression analysis, we used different cut-offs based on protein abundance, due to greater error for lower abundant proteins. The protein abundance was estimated using the total number of spectra identified for each protein. The criteria used in this analysis include a fold change $\geq$2.5 with a p-value $\leq$ 0.001 for proteins with SC $\leq$ 7, fold change $\geq$2.0 with a p-value $\leq$ 0.01 for proteins with SC between 8 and 19, fold change $\geq$2.0 with a p-value $\leq$ 0.05 for proteins with SC between 20 and 79, and a fold change $\geq$1.5 with a p-value $\leq$ 0.05 for proteins with SC 80 or higher. In addition, analysis of possible pathway networks was performed with IPA (QIAGEN Inc., https://www.qiagenbioinformatics.com/products/ingenuity-pathway-analysis) for proteins with medium and high abundancy (p-value $<$ 0.05).

2.8. Statistics analysis

Data were analyzed using GraphPad Prism v8.1.1 (GraphPad Ssoftware, La Jolla, CA) and are presented as the mean ± standard error of the mean (SEM). Two-way ANOVA with Turkey's Multiple Comparisons test and unpaired, two-tailed Student's t-test were used for determining statistical significance between groups with an alpha value of 0.05. P values $\leq$ 0.05 were considered statistically significant.

3. Results

3.1. Exposure to low-level oxidative stress in the absence of DJ-1 results in RPE and retinal degeneration

We have previously reported that lack of DJ-1 renders the RPE susceptible to increased degeneration at early time points after exposure to $NaIO_3$ when compared with C57Bl/6J (WT) control mice injected with a high dose (25 mg/kg) of this oxidizing agent [8].

Here, we analyzed the retina and RPE of both C57BL/6J (WT) and DJ-1 KO mice 7 days PI with increasing concentrations (10, 15, and 20 mg/kg) of $NaIO_3$ (Fig. 1). Initially, whole-mount RPE of 3-month-old mice were prepared, labeled with phalloidin-TRITC (Fig. 1A), and the RPE degeneration area quantified (Fig. 1C). At the lowest dose tested (10 mg/kg), no degeneration was observed in WT mice. Interestingly, in the DJ-1 KO retina, degeneration was observed but it was restricted to the area around the optic nerve head. At higher doses (15 and 20 mg/kg $NaIO_3$), RPE degeneration was seen in both DJ-1 KO and WT mice. However, the extent of degeneration was greater in the RPE of DJ-1 KO mice than in controls (Fig. 1A). Our observations indicated that following oxidative stress, the degeneration is initiated in the RPE around the optic nerve (Fig. 1A, arrows) and progresses outward towards the periphery. Injections with PBS, the vehicle control, failed to induce RPE degeneration. Quantification of the RPE degeneration area indicated 24% degeneration in DJ-1 KO mice treated with 10 mg/kg $NaIO_3$. At 15 mg/kg $NaIO_3$, 29% and 38% of the RPE was degenerated in WT and DJ-1 KO mice, respectively. At 20 mg/kg $NaIO_3$, 54% of the RPE in WT and 63% in DJ-1 KO mice was degenerated (Fig. 1C). Higher magnification observations of the whole-mount RPE confirmed the typical hexagonal RPE morphology in WT and DJ-1 KO mice injected with PBS and WT mice injected with 10 mg/kg of $NaIO_3$. The RPE of WT mice injected with 15 and 20 mg/kg of $NaIO_3$ and DJ-1 KO mice injected with 10, 15 and 20 mg/kg of $NaIO_3$ exhibited amorphous RPE cells, frequently displaying stress fibers (Supplemental Fig. S2, arrow heads) at the edge of the degenerated area (Supplemental Fig. S2, asterisks). Our observation also showed that phalloidin labeling intensity was higher in degenerated area of WT mice injected with 15 mg/kg and DJ-1 KO injected with 10 mg/kg $NaIO_3$ probably because although RPE morphology was highly abnormal, the cells were still present. In samples injected with higher doses, RPE cells had already degenerated and were cleared by infiltrating inflammatory cells.

To elucidate the role of DJ-1 in aging and low oxidative stress conditions, both 3- and 15-month-old C57BL/6J and DJ-1 KO mice were exposed to low-level oxidative stress (10 mg/kg $NaIO_3$), and their retinas analyzed 7 days PI (Fig. 1B). The retina and RPE displayed normal morphology and were comparable among both young and old WT and DJ-1 KO mice injected with PBS. When both mouse groups were injected with 10 mg/kg $NaIO_3$, RPE death and photoreceptor atrophy was observed only in DJ-1 KO retinas. Low-level oxidative stress in young and old DJ-1 KO mice resulted in significant RPE and photoreceptor degeneration, with inflammatory cells present in the subretinal space (Fig. 1B and Supplemental Fig. S3, asterisks). In contrast, WT mice displayed normal RPE and retinal morphology. Although the retinas of 15-month-old WT mice injected with $NaIO_3$ did not exhibit any degeneration, the presence of vacuoles in the RPE cytoplasm was consistently observed (Fig. 1B, arrows). Quantification of retinal damage in mice subjected to low-level oxidative resulted in 70% and 85% degeneration in 3- and 15-month-old retinas of DJ-1 KO mice, respectively, when compared to age-matched WT mice (Fig. 1D). Altogether, our results suggest that loss of DJ-1 renders the DJ-1 KO mice susceptible to oxidative stress-related damage and that aging further exacerbates these effects.

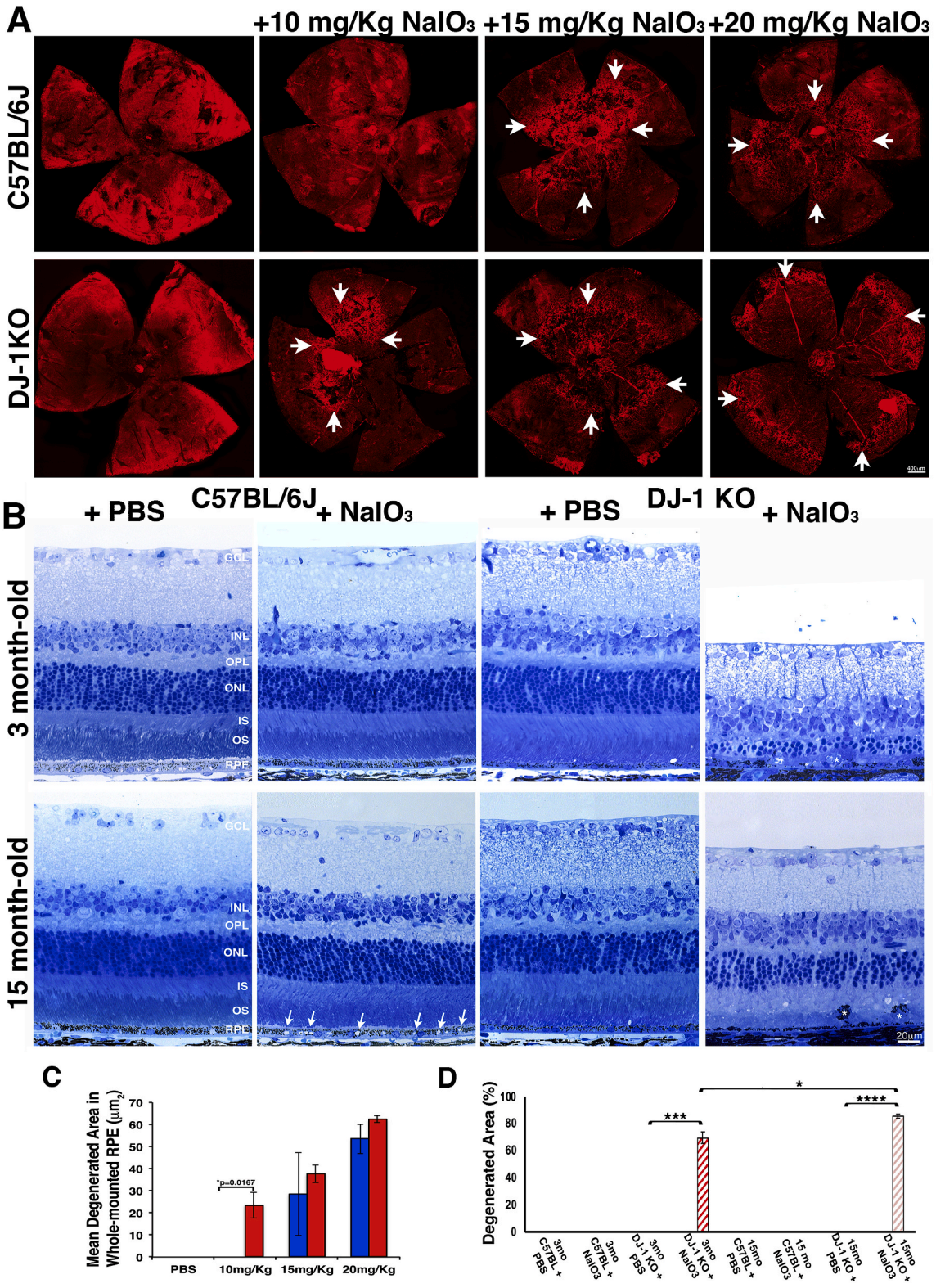

Fig. 1. Effect of sodium iodate ($NaIO_3$) on retina morphology in young and old C57BL/6J (WT) and DJ-1 knockout (KO) mice. (**A**) Representative images of RPE/choroid whole-mounts labeled with phalloidin-TRITC (red) and injected with increasing concentration of $NaIO_3$; degeneration edges are highlighted by white arrows. (**B**) Representative images of toluidine blue stained retinas of 3- month-old (young) and 15- month-old (old) WT and DJ-1 KO mice injected with PBS and $NaIO_3$. Quantification of degenerated area in young RPE/choroid whole-mounts (**C**) and whole retinas (**D**) of both young and old mice. Degeneration is expressed as mean ± SEM (n = 3–5). Unpaired, two-tailed Student's t-test was performed; *p ≤ 0.05, **p ≤ 0.01, ***p ≤ 0.001, ****p ≤ 0.000. (For interpretation of the references to colour in this figure legend, the reader is referred to the Web version of this article.)

3.2. Exposure to low-level oxidative stress and loss of DJ-1 result in "accelerated" aging retinal phenotype

Gliosis, a universal response to many retinal injuries, pathological conditions, and aging, leads to the upregulation of GFAP expression by Müller cells [16–18]. Using confocal microscopy, qualitative comparisons were pursued between the different groups of mice. In retinas of 3-month-old WT injected with PBS, GFAP labeling was seen mainly at the endfeet of Müller cells (Fig. 2A). Remarkably, the retinas of 3- month-old DJ-1 KO displayed weaker GFAP labeling than WT retinas. Exposure to low levels of oxidative stress ($NaIO_3$ 10 mg/kg) in both WT and DJ-1KO mice, resulted in enhanced GFAP labeling in Müller cells, with distribution advancing towards the inner nuclear layer along cell processes (Fig. 2A, arrowheads). Retinas from 15- month-old WT mice injected with PBS displayed stronger GFAP labeling than that of their younger counterparts. However, upon low-level oxidative stress, retinas exhibited increased GFAP labeling. Retinas of 15- month-old DJ-1 KO showed stronger GFAP labeling that their younger counterparts. However, exposure to low-level oxidative stress did not result in increased GFAP labeling possibly due to significant degeneration of the central retina.

Qualitative comparisons were also pursued between the different groups of mice after labeling with glutamine synthetase (GS), the glia-specific enzyme glutamine synthetase. In retinas of 3- month-old WT injected with PBS, GS labeling was evenly seen in the cytosol of Müller cells radial processes, extending from the inner retina at endfeet to the outer retina at the photoreceptor inner segments (Supplemental Fig. S4). Remarkably, the retinas of 3- month-old DJ-1 KO displayed visibly weaker GS labeling than WT retinas, GS labeling was seen at the endfeet of Müller cells. Exposure to low levels of oxidative stress ($NaIO_3$ 10 mg/kg) in WT resulted in decreased GS labeling and increased distribution at the endfeet of Müller cells (Supplemental Fig. S4, arrowheads) while it resulted in close to complete absence from the DJ-1 KO retinas. Retinas from 15- month-old WT mice injected with PBS displayed weaker GS labeling than that of their younger counterparts. However, upon low-level oxidative stress, retinas did not exhibit significant changes in overall GS labeling; a visible translocation of GS to the endfeet of Müller cells was observed. Retinas of 15- month-old DJ-1 KO showed stronger GS labeling than their younger counterparts. However, exposure to low-level oxidative stress decreased GS labeling, possibly due to significant degeneration of the central retina. Our results suggest that aging and low-level oxidative stress results in Müller cell gliosis, increased GFAP, and decreased GS in WT mice. Loss of DJ-1 results in overall lower levels of GFAP and GS than in young control mice retinas.

The basal surface of RPE cells attaches to Bruch's membrane (BM), a specialized and acellular layer separating the RPE from the choriocapillaris. Aging human retinas accumulate neutral lipids in their BM, as measured by labeling with Nile red, a fluorescent dye commonly used to detect deposition of neutral lipid droplets [19]. The retinas of 3-month--old WT mice injected with PBS exhibited a faint, dull red staining in the photoreceptor outer segments, RPE, and BM (Fig. 2B). In comparison, 3-month-old DJ-1 KO mice injected with PBS exhibited a continuous band of increased fluorescence intensity in the BM and spotty fluorescent intracellular lipid droplets (Fig. 2B, arrowheads), suggesting increased lipid deposition in the retinas of young DJ-1 KO mice. A similar pattern of lipid deposition was observed in 15- month-old WT and DJ-1 KO mice injected with PBS. Both 3- and 15- month-old WT mice exposed to low-level oxidative stress also showed lipid deposition. Exposure of both 3- and 15- month-old DJ-1 KO mice to low oxidative stress resulted in loss of Nile red staining likely because the RPE cells were degenerated. Quantification of this staining demonstrated an increasing trend in the number of intracellular lipid droplets in 3-month-old WT mice exposed to low-level oxidative stress, similar to baseline levels seen in 3- month-old DJ-1 KO mice injected with PBS, and during aging of both WT and DJ-1 KO mice (Fig. 2D). Significant increase in the number of lipid droplets was detected between 3-month--old DJ-1 KO and 15-month-old DJ-1 KO mice injected with PBS, and between 3-month-old WT and 15-month-old WT exposed to low oxidative stress. These results indicate that aging, low-level oxidative stress in WT mice, and DJ-1 loss lead to cellular changes reflected by the increased accumulation of neutral lipids in BM and droplets in the RPE cytoplasm.

Immunoreactivity to AGE adducts increases in the aged BM [20]. Immunoreactive labeling of the posterior retina for AGE was mostly detected at the RPE BM. The retinas of 3- and 15-month-old WT mice injected with PBS exhibited a faint dull red staining in the RPE BM (Fig. 2C). In comparison, labeling for AGE was more prominent in the BM of 3- and 15-month-old DJ-1 KO mice injected with PBS (Fig. 2C). Exposure of 3- and 15-month-old WT mice to low-level oxidative stress resulted in increased AGE accumulation in BM. Exposure of both 3- and 15- month-old DJ-1 KO mice to low oxidative stress resulted in RPE atrophy and significantly increased AGE staining in the remaining BM and degenerated area. To assess AGE accumulation in BM, we quantified the intensity of AGE immunoreactivity across the experimental groups (Fig. 2E). We detected an increasing trend for AGE staining in both 3- and 15- month-old WT and DJ-1 KO mice exposed to low-levels of oxidative stress and in 3- and 15-month-old DJ-1 KO mice injected with PBS. AGE immunoreactivity was the most significantly increased in 15-month-old DJ-1 KO mice exposed to low oxidative stress compared with all other experimental groups ($P < 0.0001$). These results indicate that low-level oxidative stress together with DJ-1 loss lead to increased accumulation of AGEs in BM. Altogether, our results suggest that during aging, the retina undergoes gliosis as well as accumulation of neutral lipids and AGEs in the RPE. Moreover, low-level oxidative stress in WT mice and DJ-1 loss alone can trigger changes similar to those observed during aging but with reduced magnitudes.

3.3. Exposure of young mice to low-level oxidative stress results in antioxidant gene expression changes similar to that of aging

Following oxidative stress, DJ-1 binds to various transcription factors to activate different cellular pathways involved in the fight against this insult. Under these circumstances, DJ-1 acts as a coactivator or corepressor that regulates its target genes [21]. We measured the transcript levels of antioxidant enzymes previously reported to be affected by DJ-1, including: superoxide dismutase 1 and 2 (*Sod1* and *Sod2*); peroxiredoxin 1 (*Prdx1*); glutathione transferases pi1 (*Gstp1*); glutathione peroxidase (*Gpx1*); nuclear factor erythroid 2-related factor 2 (*Nrf2*) and its downstream target NAP(D)H quinone1 (*Nqo1*) and heme oxygenase1 (*Hmox1*) (Fig. 3). With aging, we observed no significant changes in the expression of these genes in the retina of WT mice. In the retina of 15- month-old DJ-1 KO mice, only *Nrf2*, *Sod1*, *Sod2*, and *Gstp1* were significantly upregulated compared with that of their younger counterparts. Intriguingly, the baseline level of these antioxidant genes was downregulated in 3-month-old DJ-1 KO mice compared with age-matched WT mice (Fig. 3A). We also observed a significant upregulation of *Park7* (DJ-1) and an increasing trend for all tested genes in WT mice RPE upon aging (Fig. 3B). Moreover, *Nrf2*, *Sod1*, *Sod2*, *Nqo1*, *Prdx1*, and *Gpx1* were significantly downregulated in the RPE of 15-month old DJ-1 KO mice compared with their 3- month old counterparts and significantly upregulated in 3-month-old DJ-1 KO mice compared with age-matched WT mice (Fig. 3B). Exposure to low-level oxidative stress resulted in significant upregulation of *Nrf2*, *Sod1*, *Sod2*, *Prdx1* and *Park7* in the retina of 3-month-old WT mice, while *Sod1*, *Nqo1*, *Hmox1*, *Prdx1*, and *Gstp1* were significantly upregulated in 3-month-old DJ-1 KO mice (Fig. 3C). In contrast, exposure to low-level oxidative stress resulted in significant upregulation of only the *Park7* gene in 3-month-old WT mice, while *Nrf2*, *Sod1*, *Sod2*, *Nqo1*, *Prdx1*, and *Gpx1* were significantly downregulated from baseline levels in the RPE of 3-month-old DJ-1 KO mice (Fig. 3D). In 15-month-old mice, among all the genes screened only *Gstp1* was significantly downregulated in the retinas of DJ-1 KO mice (Fig. 3E) whereas, *Nrf2*, *Gpx1*, and *Park7* were significantly upregulated in the RPE of WT mice treated with $NaIO_3$

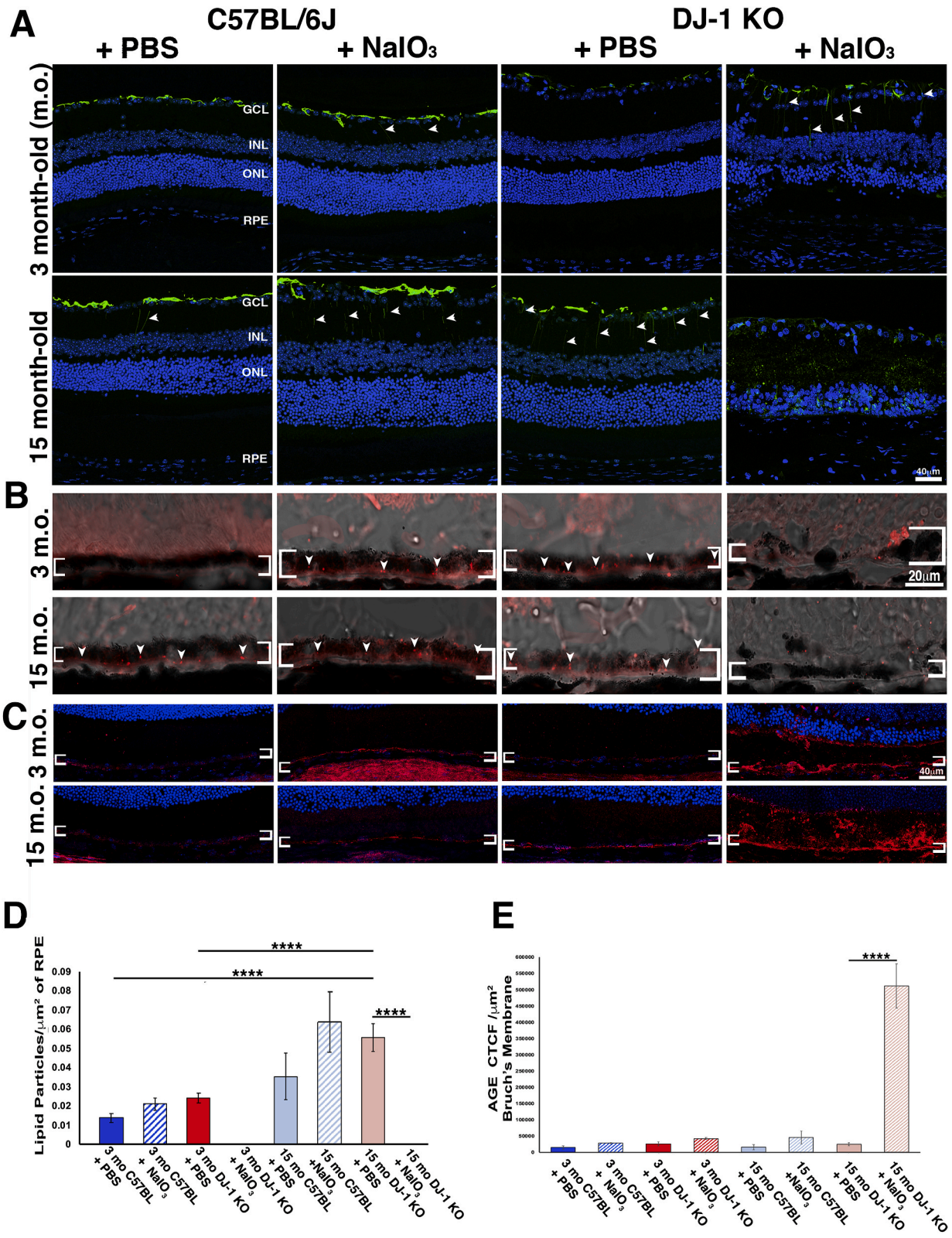

Fig. 2. Expression of retinal markers during aging and under low-level oxidative stress (10 mg/kg $NaIO_3$). Representative images of young and old retinas from WT and DJ-1 KO mice injected with PBS or $NaIO_3$ and stained for anti-glial fibrillary acidic protein (GFAP) (**A**), Nile Red dye for neutral lipids (**B**) and advanced glycation end products (AGEs) (**C**). Quantification of Nile Red stained neutral lipid droplets in RPE (**D**) and AGEs in Bruch's membrane (**E**) of young and old WT and DJ-1 KO mice. The apical and basal borders of the RPE is highlighted by brackets in **B** and **C**. Data are represented as mean ± SEM; n = 3–4 mice per group. Two-way Anova with Tukey's multiple comparisons test was performed; ****$p \leq 0.0001$. (For interpretation of the references to colour in this figure legend, the reader is referred to the Web version of this article.)

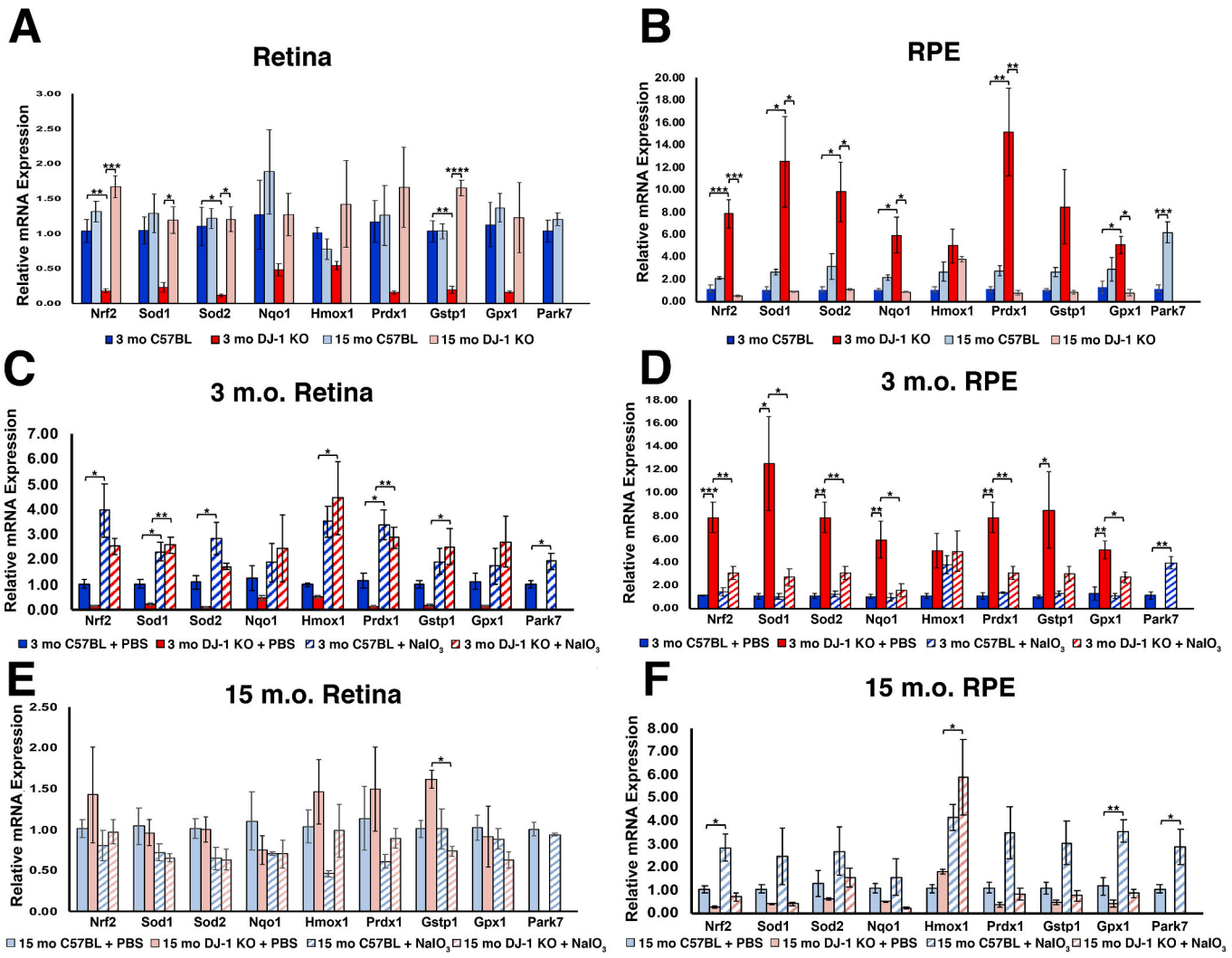

Fig. 3. Transcriptional changes in retina and RPE due to aging and low-level oxidative stress (10 mg/kg $NaIO_3$). Quantitative RT-PCR analysis of *Nrf2*, *Sod1*, *Sod2*, *Nqo1*, *Hmox1*, *Prdx1*, *Gstp1*, *Gpx1* and *Park7* (DJ-1) in the retina (**A**) and RPE (**B**) of young and old WT and DJ-1 KO mice; the retina of young (**C**) and old (**E**) WT and DJ-1 KO mice with or without $NaIO_3$ treatment; and the RPE of young (**D**) and old (**F**) WT and DJ-1 KO mice with or without $NaIO_3$ treatment. Data are represented as mean ± SEM; n = 3–4 per group. Two-way Anova with Tukey's multiple comparisons test was performed; *p ≤ 0.05, **p ≤ 0.01, ***p ≤ 0.001, ****p ≤ 0.0001.

(Fig. 3F). Altogether, the upregulation of antioxidative genes in RPE of DJ-1 KO mice implies that these cells are under oxidative stress in the absence of DJ-1/*Park7*. In addition, our data suggests that antioxidant response capacity of the retina diminishes with aging in both WT and DJ-1 KO mice.

3.4. Aging and DJ-1 absence result in changes in antioxidant proteins

We carried out western blot analysis to determine antioxidant enzymes levels and further understand our gene expression findings (Fig. 4). In the aging WT retina, we observed increased DJ-1 levels in the lysates. Meanwhile, DJ-1 KO mouse retinas displayed age-related increases in both oxidized and reduced SOD1 as well as decreased PRDX1 levels (Fig. 4A and B). The levels of oxidized SOD1 and PRDX1 were significantly upregulated in DJ-1 KO retinas and RPE compared with their 3- month old counterparts (Fig. 4C and D).

We next analyzed the NRF2 labeling in retinal cryosections (Supplemental Fig. S5) and detected an increasing trend in NRF2 levels in aged retinas. Exposure to low-level oxidative stress resulted in an increase in NRF2 signal intensity in young WT retinas and a decrease in DJ-1 KO retinas. Although not statistically significant, these results mirrored our transcriptional analysis results of the WT retina and DJ-1 KO RPE.

Moreover, our proteomics analysis identified proteins expressed in the retina and RPE of 3- month-old WT and DJ-1 KO injected with PBS. Analysis of possible pathway networks identified mitochondria dysfunction as one of the top canonical pathways affecting both the retina and RPE of the DJ-1 KO mice. However, the magnitude of dysfunction was much higher in the RPE of DJ-1 KO compared with WT mice (Supplemental Table 3). The list of affected proteins is provided in Supplemental Table 4.

4. Discussion

The free radical theory of aging states that the process of aging is, at least in part, due to the accumulated damage inflicted by free radicals and reactive oxygen species (ROS)-mediated oxidative stress [1]. DJ-1 is a multifunctional protein that plays an essential role in the oxidative stress response in several diseases, including early-onset and sporadic PD and neurodegenerative disorders such as amyotrophic lateral sclerosis, Alzheimer's disease, and Huntington's disease. We previously reported for the first time the antioxidant protection provided by DJ-1 in

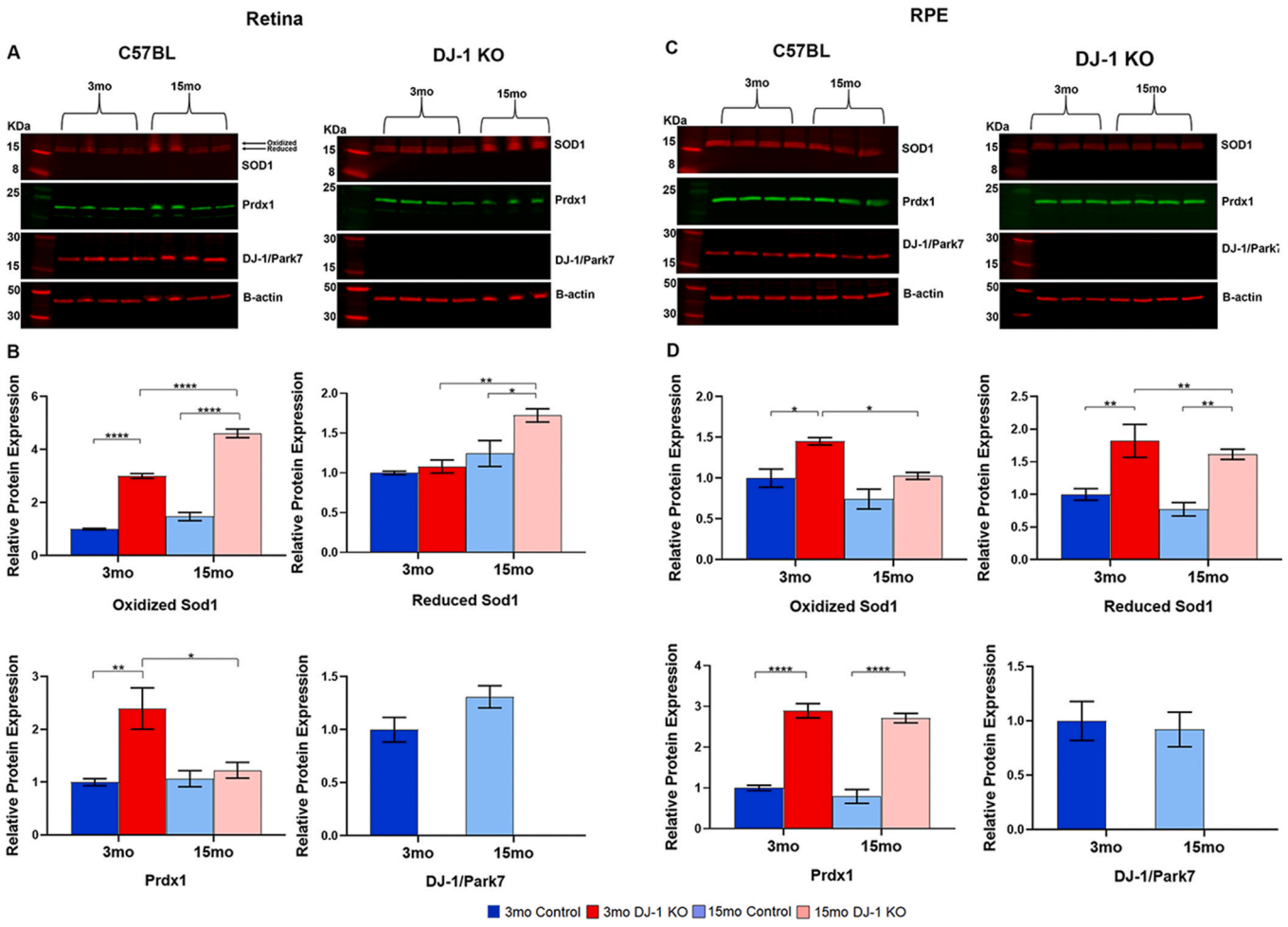

Fig. 4. Antioxidant protein changes in retina and RPE due to aging. Western blot analysis for SOD1, PRDX1 and PARK7 (DJ-1) in retina (**A**) and RPE (**C**) of young and old WT and DJ-1 KO mice. Quantification of protein signal from western blots in retina (**B**) and RPE (**D**) of young and old WT and DJ-1 KO mice. Data are represented as mean ± SEM; n = 3–4 mice per group. Two-way ANOVA with Tukey's multiple comparisons test was performed; *p ≤ 0.05, **p ≤ 0.01, ***p ≤ 0.001, ****p ≤ 0.0001.

RPE cells *in vitro* [22] and in the retina of DJ-1 KO mice *in vivo* [8,11]. Here, we systematically examined the role of DJ-1 in the retina and RPE during aging and found that low-level oxidative stress 1) mimics aging changes in the retina and RPE of WT mice and, 2) results in retinal degeneration in DJ-1 KO mice, independent of age. Likewise, loss of DJ-1 alone results in "accelerated aging" of the young RPE in terms of increased neutral lipids accumulation and AGEs deposition and intermediate between young WT RPE subjected to low-oxidative stress and aged WT RPE. These findings are summarized in Fig. 5.

We extended our previous observations by exposing WT and DJ-1 KO mice of different ages to increasing concentrations of the oxidizing agent $NaIO_3$. This model has been previously used to study retinal degeneration in different species because the degeneration resembles some of the features of AMD [23]. Our dose-dependent experiments on young mice confirmed our previous observations that the absence of DJ-1 renders mice susceptible to $NaIO_3$ (Fig. 1A) [8]. At the low dose of 10 mg/kg $NaIO_3$, the RPE was preferentially degenerated in DJ-1 KO mice but not in WT mice. This result is consistent with a previous study in which little to no changes were observed in the RPE of C57BL/6J mice at same dose [24].

Using the 10 mg/kg low dose, we expanded our investigations to further identify the role of DJ-1 in the antioxidant machinery of the RPE and retina during aging (Fig. 1B). DJ-1 KO mice were prone to low-dose $NaIO_3$-mediated oxidative damage irrespective of age. These observations indicate that loss of DJ-1 expression renders the RPE unable to metabolize and combat low-level oxidative stress. Our results draw a parallel to the retinal degeneration observed in AMD, where the occurrence of genetic variants may render the retina and RPE unable to fight sustained, low-levels of oxidative stress.

Significant age-related changes were detected in both mouse strains when probed with aging and oxidative stress markers, namely AGEs, GFAP, and Nile red (Fig. 2). Astrocytes constitutively express GFAP, while mature radial glia Müller cells usually do not express GFAP [25,26]. Reactivation of Müller cells, also called gliosis, is characterized by upregulated expression of the intermediate filament GFAP. This change is an indicator of stress and a universal response to aging and many retinal pathological conditions [16–18].

In comparison, low-level oxidative stress in WT mice resulted in no retinal degeneration at either age, although GFAP expression increased with distribution advancing towards the inner nuclear layer through cell processes (Fig. 2A). These results suggest that low oxidative stress to some extent mimic aging in term of GFAP up-modulation. Surprisingly, in young DJ-1 KO retinas, low levels of GFAP were observed at the endfeet of Müller cells, but then increased with aging. One possible explanation could be that DJ-1 regulates GFAP expression, and thus GFAP expression is deregulated in the absence of DJ-1. Indeed, recent studies have established that DJ-1 regulates GFAP expression in brain astroglia through STAT3 and SOX9 [27,28]. Alternatively, the DJ-1 KO retina may be depleted or deficient in cytokines such as interleukin-1β [29] and ciliary neurotrophic factor [30], which have been shown to

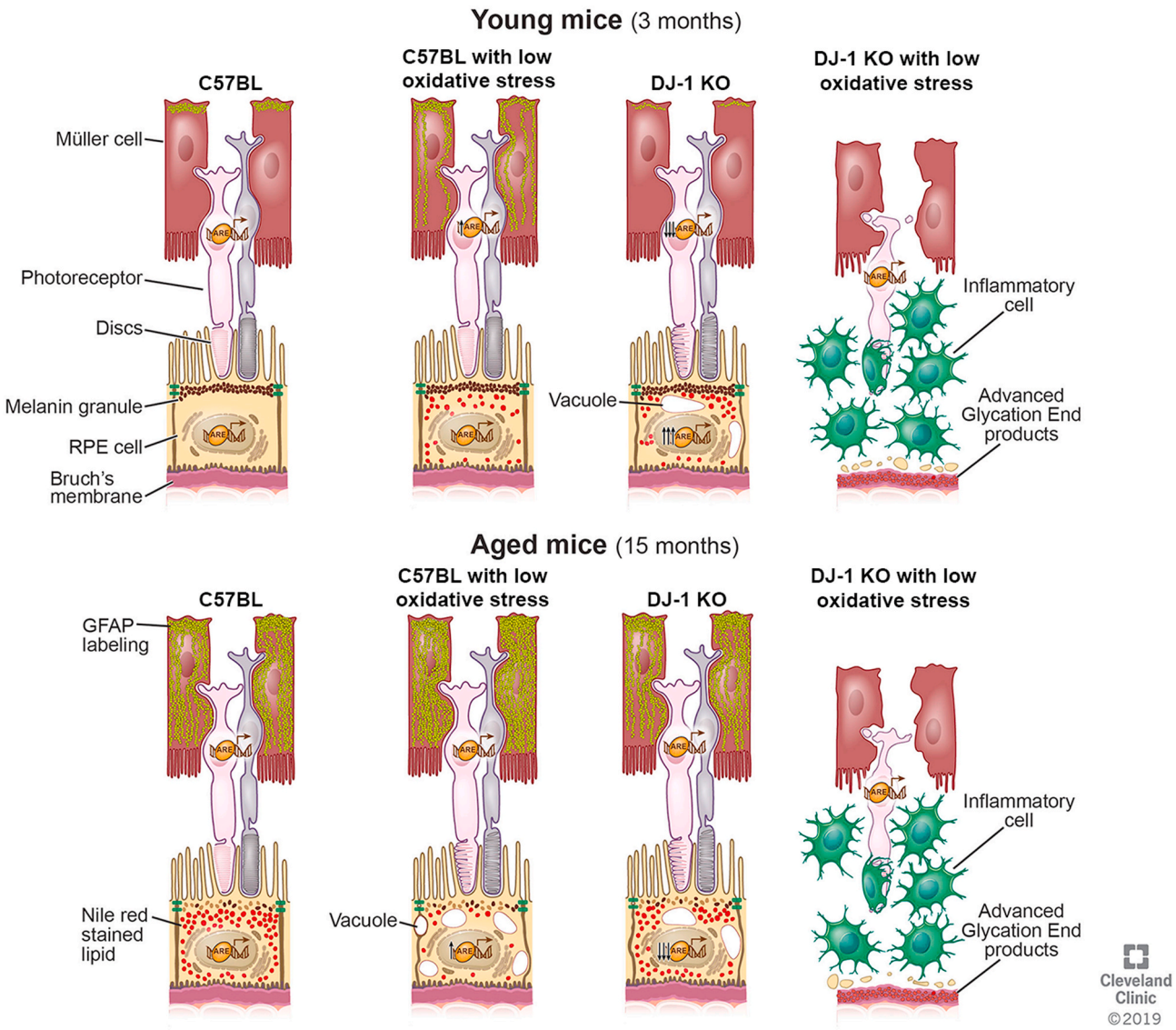

Fig. 5. Schematic model of the role of aging and DJ-1 in the regulation of oxidative stress responses in the RPE and retina. Aging and low-level oxidative stress resulted in no visible degeneration, increased GFAP, and Nile red labeling in WT retinas. However, aging results in increased GFAP and Nile red labeling in DJ-1 KO retinas, while low-level oxidative stress results in retinal degeneration, decreased Nile red, and increased AGEs in the DJ-1 KO retinas. In young mice, expression levels of antioxidant genes were significantly upregulated in the RPE, but downregulated in the retina, of DJ-1 KO mice compared with WT mice. In old mice, expression levels of these genes were significantly downregulated in RPE, but remained unchanged in the retina, of DJ-1 KO mice compared with WT mice. In young mice, low-level oxidative stress upregulated gene expression in the retina of both mice. In young RPE, the majority of genes were not significantly altered in WT mice but were significantly downregulated in DJ-1 KO mice. In old mice, low-level oxidative stress resulted in no modulation of antioxidant gene expression in the retina. Meanwhile, a few of the genes were upregulated in the RPE of WT but not DJ-1 KO mice. (Reprinted with the permission of the Cleveland Clinic Center for Medical Art & Photography © 2019. All Rights Reserved). (For interpretation of the references to colour in this figure legend, the reader is referred to the Web version of this article.)

regulate GFAP expression in retinal Müller cells.

The enzyme glutamine synthetase (GS) is involved in the glutamate/glutamine cycle that catalyses the convertion of glutamate into glutamine in the Müller cells. The expression of GS is regulated by glutamate [31,32], at least partially by growth factors such as the basic fibroblast growth factor (bFGF) [33] and by the availability of ammonia [34]. The expression of GS in Müller cells is reduced when the photoreceptors, the major glutamate-releasing neuronal population are degenerated in inherited pathological conditions such as hereditary disease, light damage, retinal detachment, under ischemic, inflammatory, and traumatic conditions in the retina [32,35]. In WT mice exposed to low-level oxidative stress we observed the translocation of GS within the Müller cells, towards their endfeet in the ganglion cell layer, where the injured ganglion cells likely release excess glutamate (Supplemental Fig. S4). This observation is similar to previous reports on the analysis of retinas after optic nerve crush [36]. In addition, the overall levels of GS were also decreased in mice exposed to low-level oxidative stress. Previous studies reported GS inactivation by oxidative stress and decreased GS expression in retinas exposed to increased oxidative stress [37–41]. Aged WT retinas displayed decreased GS labeling; it suggests that aged photoreceptors are dysfunctional. To our knowledge this is the first observation of GS expression in the aging retina. The decreased levels of GS observed in the young DJ-1 KO retina may be related to dysfunctional photoreceptors. Indeed, our previous work reported notably decreased immunocytochemical staining for both red/green opsin and rhodopsin in retinal sections of 18 month-old control around the optic nerve region [11]. Further experiments are needed to better understand the increased presence of GS in aged DJ-1 KO retinas.

Deposition of neutral lipids and AGEs underneath the RPE accumulates during aging and is known to contribute to age-related maculopathies [19,20]. We thus analyzed neutral lipids by labeling samples with Nile red. A clear trend of age-related, increased staining was observed in WT and DJ-1 KO RPE, with DJ-1 KO mice showing increased accumulation of neutral lipids in the RPE cytoplasm and BM compared with that of WT mice. This labeling pattern in DJ-1 KO mice was similar to WT mice exposed to low-level oxidative stress (Fig. 2B and D). Thus, DJ-1 loss possibly alters lipid metabolism in RPE cells and results in a phenotype consistent with "early" or "accelerated" aging in terms of neutral lipid accumulation within the RPE.

Indeed, a recent study reported on DJ-1 regulation of flotilin-1 and caveolin-1 stability with resulting alterations in cellular cholesterol level, membrane fluidity, and lipid raft-dependent endocytosis of astrocytes [42]. In addition, a different study reported that low-density lipoprotein receptor (LDLR) gene expression is altered in DJ-1 KO cells [43]. The same group subsequently reported that DJ-1 stimulates LDLR gene expression at the transcriptional level by associating with SREBP and affects serum LDL cholesterol levels in male mice [44].

A synergism exists between AGEs and oxidative stress, where AGEs lead to ROS generation and, oxidative stress promotes AGE production. Our understanding of the consequences of AGE accumulation in tissues is not fully clear; however, these glycoxidation products cause protein cross-linking, reduced solubility, enzymatic dysfunction, and loss of receptor recognition [45]. Postmortem human eyes exhibit increased AGEs in the RPE during aging or pathological conditions such as AMD [20]. Here, mice of both strains and ages exposed to low-levels of oxidative stress showed an increasing trend of elevated AGE, but AGEs were significantly elevated only in the BM of old DJ-1 KO mice (Fig. 2C and E). These results indicate an association between increased oxidative stress and retinal degeneration with accumulation of AGEs in the RPE BM.

The retina and RPE exhibit structural changes during aging. The retina displays thinning due to neuron loss and shortening of photoreceptors. The RPE displays loss of melanin granules, an increase in the number of residual bodies, accumulation of the age pigment lipofuscin, accumulation of basal deposits on or within BM, the formation of drusen, thickening of BM, atrophy of apical microvilli, and disorganization of basal infoldings [46]. Increased oxidative stress and a general decline of essential functions lead to cellular events that in turn induce several of these age-related changes. Previous studies characterizing the differences between young adult and aged RPE samples have shown through different experimental approaches that proteins involved in antioxidation are one of several cellular functions explicitly affected by aging [47,48]. In the present study, no significant changes in the expression of antioxidant genes were identified in WT mice during both retina and RPE aging. However, exposure to low-level oxidative stress resulted in significant upregulation of several antioxidants in the young retina and aged RPE of WT mice (Fig. 3). Our results agree with a previous study where treatment of young mice with $NaIO_3$ significantly increased GCLM, HO1, and NQO expression; in contrast, $NaIO_3$ failed to increase transcript levels of these Nrf2 downstream target genes in older mice [49].

Upon exposure to stress oxidative conditions, DJ-1/PARK7 is translocated into the nucleus to cytoprotect neurons and other cells. The protein does not exhibit any distinct DNA-binding domains suggesting it likely acts as a co-activator that regulates the activity of transcription factors such as p53, polypyrimidine tract-binding protein-associated splicing factor (PSF), KEAP-1, and NRF-2, among others. Therefore, the loss of activation of DJ-1 leads to the onset of neurodegenerative diseases such as PD while excessive activation of DJ-1 leads to cancer [44]. In this study, we found that DJ-1 loss alone in the RPE precipitates into the augmented oxidative load of the cell at a young age. The opposite was observed in DJ-1 KO retinas of young mice with diminished expression of antioxidant genes (Fig. 3A and B). The opposing modulation of the antioxidant genes of the retina and RPE of DJ-1 KO mice could be related to the changes in cell-specific metabolism. Metabolically, retinas rely mostly on aerobic glycolysis, while RPE cells depend more on mitochondria [50,51]. This hypothesis is supported by our own proteomic analysis of the proteins present in the retina and RPE of 3-month-old WT and DJ-1 KO mice injected with PBS, which displayed higher mitochondria dysfunction in the RPE of the DJ-1 KO when compared with WT mice (Supplemental Tables S3 and S4).

We further found that during aging and when the basal elevated oxidative load is further supplemented with low-level oxidative stress in young DJ-1 KO mice, the antioxidant machinery in RPE is unable to maintain elevated antioxidant gene expression, resulting in their decreased expression (Fig. 3B and D). This decrease may also be related to the observed RPE atrophy in the central retina. Previous studies have shown that DJ-1 regulates the expression of *Sod1*, *Sod2*, *Sod3*, *Nrf2*, and *Nrf2* target genes via conserved antioxidant response elements such as Nqo1 and Hmox-1 [52–54]. The majority of studies performed using cell cultures reported transcription of these genes directly related to the level of DJ-1 expression. However, antioxidant genes and proteins were also upregulated under increased oxidative stress and in the absence of DJ-1 [53,55]. Moreover, a different DJ-1−/− mouse line displayed increased *Sod2* expression in the brain [56]. Thus, the elevated levels of antioxidant genes in the RPE of DJ-1 KO mice may be a result of these cells being under stress due to the loss of DJ-1 and its effects on RPE metabolism.

We previously analyzed the protein profile of young (3- 4-month-old) and aged (24-25-month-old) RPE from rats and identified SOD1, SOD2, DJ-1, PRDX1, PRDX2, PRDX3, PRDX4, PRDX6, GSTP1, GPX1, GPX3, and GPX4 among proteins with antioxidant function that were present in aged RPE [9]. Here, we measured only SOD1, PRDX, and DJ-1 levels, because of the unavailability of suitable antibodies for other genes studied at the transcript level, and detected increased oxidized SOD1, PRDX1, and DJ-1 levels in the aged WT retinas (Fig. 4). This agrees with our previous findings of increased DJ-1 levels in aged retinas [9]. Moreover, previous studies described SOD1 migration via SDS/PAGE as a closely spaced doublet [57,58] and identified the upper protein signal as an oxidized form of SOD1. However, the biological significance of these two bands remains unresolved. We further analyzed NRF2 levels in labeled cryosections but found no significant changes in NRF2 signals, although trends were observed (Supplemental Fig. S5). As previously determined [11], we also detected decreased NRF2 levels in DJ-1 KO retinas. As DJ-1 prevents NRF2 interaction with its inhibitor protein KEAP-1, absence of DJ-1 results in decreased NRF2 levels under baseline conditions. In a cellular context of overall low NRF2 levels, cells would be more susceptible to damage by oxidative stress. Thus, under low-level oxidative stress, WT but not DJ-1 KO RPE cells were able to upregulate Nrf2 transcripts and proteins to fight the stress.

The present study demonstrated that low-level oxidative stress mimics aging in WT retinas and RPE. In the absence of DJ-1 and cellular stress or environmental insults, the RPE and photoreceptor cells can survive but they may not fulfill all normal functions and they display early signs of cellular stress similar to some degree to age-related changes. When these cells are exposed to low-level oxidative stress, DJ-1 is required to attenuate the stress or activate stress response pathways. Thus, RPE and photoreceptor cells deficient in DJ-1 are more susceptible to insults such as $NaIO_3$ exposure and are prone to degenerate. In this context, the DJ-1 KO model draws a parallel to AMD pathology, where the occurrence of one of the several genetic variants reported, results in chronic low-level oxidative stress. Future studies further detailing the DJ-1-related defects in RPE cells will possibly broaden our understanding of the AMD pathology.

Data availability

The data that support the findings of this study are available in DryAd at https://datadryad.org/stash/share/GtpGnyVJV4bBVtWK5xu-IDwfhOEW6vlndr-5HKdXtWM from the corresponding author

upon request.

Author contributions

VLB and MU designed the experiments and wrote the manuscript. All authors performed experiments.

Funding

This work was supported by the National Eye Institute of the National Institutes of Health [grant number R01EY027750]; a National Eye Institute P30 Core Grant [P30EY025585]; a challenge grant from the Research to Prevent Blindness; and Cleveland Clinic Foundation startup funds.

Declaration of competing interest

The authors declare no conflict of interest with the research presented in the manuscript.

Acknowledgements

The Oribtrap Elite instrument was purchased via an NIH shared instrument grant, 1S10RR031537-01. The authors thank Dr. Belinda Willard and the staff of the LRI Proteomics and Metabolomics Core for proteomics support. The authors also thank David Schumick for preparation of the illustrations.

Appendix A. Supplementary data

Supplementary data to this article can be found online at https://doi.org/10.1016/j.redox.2020.101623.

References

[1] D. Harman, Aging: a theory based on free radical and radiation chemistry, J. Gerontol. 11 (1956) 298–300, https://doi.org/10.1093/geronj/11.3.298.
[2] B.N. Ames, M.K. Shigenaga, T.M. Hagen, Oxidants, antioxidants, and the degenerative diseases of aging, Proc. Natl. Acad. Sci. U. S. A. 90 (1993) 7915–7922, https://doi.org/10.1073/pnas.90.17.7915.
[3] S. Agarwal, R.S. Sohal, Relationship between susceptibility to protein oxidation, aging, and maximum life span potential of different species, Exp. Gerontol. 31 (1996) 365–372, https://doi.org/10.1016/0531-5565(95)02039-x.
[4] Y. Nishimura, H. Hara, M. Kondo, S. Hong, T. Matsugi, Oxidative stress in retinal diseases, Oxid. Med. Cell. Longev. 2017 (2017) 4076518, https://doi.org/10.1155/2017/4076518.
[5] P.X. Shaw, T. Stiles, C. Douglas, D. Ho, W. Fan, H. Du, et al., Oxidative stress, innate immunity, and age-related macular degeneration, AIMS Mol. Sci. 3 (2016) 196–221, https://doi.org/10.3934/molsci.2016.2.196.
[6] T. Taira, Y. Saito, T. Niki, S.M. Iguchi-Ariga, K. Takahashi, H. Ariga, DJ-1 has a role in antioxidative stress to prevent cell death, EMBO Rep. 5 (2004) 213–218, https://doi.org/10.1038/sj.embor.7400074.
[7] P.J. Kahle, J. Waak, T. Gasser, DJ-1 and prevention of oxidative stress in Parkinson's disease and other age-related disorders, Free Radic. Biol. Med. 47 (2009) 1354–1361, https://doi.org/10.1016/j.freeradbiomed.2009.08.003.
[8] V.L. Bonilha, B.A. Bell, M.E. Rayborn, X. Yang, C. Kaul, G.H. Grossman, et al., Loss of DJ-1 elicits retinal abnormalities, visual dysfunction, and increased oxidative stress in mice, Exp. Eye Res. 139 (2015) 22–36, https://doi.org/10.1016/j.exer.2015.07.014.
[9] X. Gu, N.J. Neric, J.S. Crabb, J.W. Crabb, S.K. Bhattacharya, M.E. Rayborn, et al., Age-related changes in the retinal pigment epithelium (RPE), PloS One 7 (2012), e38673, https://doi.org/10.1371/journal.pone.0038673.
[10] M.R. Bohm, S. Mertsch, S. Konig, T. Spieker, S. Thanos, Macula-less rat and macula-bearing monkey retinas exhibit common lifelong proteomic changes, Neurobiol. Aging 34 (2013) 2659–2675, https://doi.org/10.1016/j.neurobiolaging.2013.04.020.
[11] V.L. Bonilha, B.A. Bell, M.E. Rayborn, I.S. Samuels, A. King, J.G. Hollyfield, et al., Absence of DJ-1 causes age-related retinal abnormalities in association with increased oxidative stress, Free Radic. Biol. Med. 104 (2017) 226–237, https://doi.org/10.1016/j.freeradbiomed.2017.01.018.
[12] C. Xin-Zhao Wang, K. Zhang, B. Aredo, H. Lu, R.L. Ufret-Vincenty, Novel method for the rapid isolation of RPE cells specifically for RNA extraction and analysis, Exp. Eye Res. 102 (2012) 1–9, https://doi.org/10.1016/j.exer.2012.06.003.
[13] M. Kinter, N.E. Sherman, in: D.M. Desiderio, N.M.M. Nibbering (Eds.), Protein Sequencing and Identification Using Tandem Mass Spectrometry, Wiley, New York, NY, 2005, https://doi.org/10.1002/0471721980.
[14] J. Cox, N. Neuhauser, A. Michalski, R.A. Scheltema, J.V. Olsen, M. Mann, Andromeda: a peptide search engine integrated into the MaxQuant environment, J. Proteome Res. 10 (2011) 1794–1805, https://doi.org/10.1021/pr101065j.
[15] J. Cox, M.Y. Hein, C.A. Luber, I. Paron, N. Nagaraj, M. Mann, Accurate proteome-wide label-free quantification by delayed normalization and maximal peptide ratio extraction, termed MaxLFQ, Mol. Cell. Proteomics 13 (2014) 2513–2526, https://doi.org/10.1074/mcp.M113.031591.
[16] J.M. Ramirez, A.I. Ramirez, J.J. Salazar, R. de Hoz, A. Trivino, Changes of astrocytes in retinal ageing and age-related macular degeneration, Exp. Eye Res. 73 (2001) 601–615, https://doi.org/10.1006/exer.2001.1061.
[17] G.P. Lewis, S.K. Fisher, Up-regulation of glial fibrillary acidic protein in response to retinal injury: its potential role in glial remodeling and a comparison to vimentin expression, Int. Rev. Cytol. 230 (2003) 263–290, https://doi.org/10.1016/s0074-7696(03)30005-1.
[18] K.H. Wu, M.C. Madigan, F.A. Billson, P.L. Penfold, Differential expression of GFAP in early v late AMD: a quantitative analysis, Br. J. Ophthalmol. 87 (2003) 1159–1166, https://doi.org/10.1136/bjo.87.9.1159.
[19] M. Rudolf, C.A. Curcio, Esterified cholesterol is highly localized to Bruch's membrane, as revealed by lipid histochemistry in wholemounts of human choroid, J. Histochem. Cytochem. 57 (2009) 731–739, https://doi.org/10.1369/jhc.2009.953448.
[20] J.T. Handa, N. Verzijl, H. Matsunaga, A. Aotaki-Keen, G.A. Lutty, J.M. te Koppele, et al., Increase in the advanced glycation end product pentosidine in Bruch's membrane with age, Invest. Ophthalmol. Vis. Sci. 40 (1999) 775–779.
[21] A. Biosa, F. Sandrelli, M. Beltramini, E. Greggio, L. Bubacco, M. Bisaglia, Recent findings on the physiological function of DJ-1: beyond Parkinson's disease, Neurobiol. Dis. 108 (2017) 65–72, https://doi.org/10.1016/j.nbd.2017.08.005.
[22] K.G. Shadrach, M.E. Rayborn, J.G. Hollyfield, V.L. Bonilha, DJ-1-dependent regulation of oxidative stress in the retinal pigment epithelium (RPE), PloS One 8 (2013), e67983, https://doi.org/10.1371/journal.pone.0067983.
[23] S.E. Nilsson, B. Knave, H.E. Persson, Changes in ultrastructure and function of the sheep pigment epithelium and retina induced by sodium iodate. I. The ultrastructure of the normal pigment epithelium of the sheep, Acta Ophthalmol. 55 (1977) 994–1006, https://doi.org/10.1111/j.1755-3768.1977.tb05681.x.
[24] J. Wang, J. Iacovelli, C. Spencer, M. Saint-Geniez, New insights on sodium iodate-induced retianl degeneration, Faseb. J. 27 (2013) 15, https://doi.org/10.4103/1673-5374.147927.
[25] A. Bringmann, T. Pannicke, J. Grosche, M. Francke, P. Wiedemann, S.N. Skatchkov, et al., Muller cells in the healthy and diseased retina, P Prog. Retin Eye Res. 25 (2006) 397–424, https://doi.org/10.1016/j.preteyeres.2006.05.003.
[26] M.V. Sofroniew, H.V. Vinters, Astrocytes: biology and pathology, Acta Neuropathol. 119 (2010) 7–35, https://doi.org/10.1007/s00401-009-0619-8.
[27] D.J. Choi, J.H. Eun, B.G. Kim, I. Jou, S.M. Park, E.H. Joe, A Parkinson's disease gene, DJ-1, repairs brain injury through Sox9 stabilization and astrogliosis, Glia 66 (2018) 445–458, https://doi.org/10.1002/glia.23258.
[28] D.J. Choi, J.K. Kwon, E.H. Joe, A Parkinson's disease gene, DJ-1, regulates astrogliosis through STAT3, Neurosci. Lett. 685 (2018) 144–149, https://doi.org/10.1016/j.neulet.2018.08.025.
[29] F.I. Baptista, C.A. Aveleira, A.F. Castilho, A.F. Ambrosio, Elevated glucose and interleukin-1beta differentially affect retinal microglial cell proliferation, Mediat. Inflamm. 2017 (2017) 4316316, https://doi.org/10.1155/2017/4316316.
[30] Y. Wang, S.B. Smith, J.M. Ogilvie, D.J. McCool, V. Sarthy, Ciliary neurotrophic factor induces glial fibrillary acidic protein in retinal Muller cells through the JAK/STAT signal transduction pathway, Curr. Eye Res. 24 (2002) 305–312, https://doi.org/10.1076/ceyr.24.4.305.8408.
[31] F. Shen, B. Chen, J. Danias, K.C. Lee, H. Lee, Y. Su, et al., Glutamate-induced glutamine synthetase expression in retinal Muller cells after short-term ocular hypertension in the rat, Invest. Ophthalmol. Vis. Sci. 45 (2004) 3107–3112, https://doi.org/10.1167/iovs.03-0948.
[32] A. Bringmann, T. Pannicke, B. Biedermann, M. Francke, I. Iandiev, J. Grosche, et al., Role of retinal glial cells in neurotransmitter uptake and metabolism, Neurochem. Int. 54 (2009) 143–160, https://doi.org/10.1016/j.neuint.2008.10.014.
[33] Y. Kruchkova, I. Ben-Dror, A. Herschkovitz, M. David, A. Yayon, L. Vardimon, Basic fibroblast growth factor: a potential inhibitor of glutamine synthetase expression in injured neural tissue, J. Neurochem. 77 (2001) 1641–1649, https://doi.org/10.1046/j.1471-4159.2001.00390.x.
[34] P. Marcaggi, M. Jeanne, J.A. Coles, Neuron-glial trafficking of NH4+ and K+: separate routes of uptake into glial cells of bee retina, Eur. J. Neurosci. 19 (2004) 966–976, https://doi.org/10.1111/j.0953-816x.2004.03165.x.
[35] A. Bringmann, A. Grosche, T. Pannicke, A. Reichenbach, GABA and glutamate uptake and metabolism in retinal glial (muller) cells, Front. Endocrinol. 4 (2013) 48, https://doi.org/10.3389/fendo.2013.00048.
[36] H. Chen, A.J. Weber, Expression of glial fibrillary acidic protein and glutamine synthetase by Muller cells after optic nerve damage and intravitreal application of brain-derived neurotrophic factor, Glia 38 (2002) 115–125, https://doi.org/10.1002/glia.10061.
[37] R.L. Levine, Oxidative modification of glutamine synthetase. I. Inactivation is due to loss of one histidine residue, J. Biol. Chem. 258 (1983) 11823–11827.
[38] G. Gomez-Baena, J. Diez, J.M. Garcia-Fernandez, S. El Alaoui, L. Humanes, Regulation of glutamine synthetase by metal-catalyzed oxidative modification in the marine oxyphotobacterium Prochlorococcus, Biochim. Biophys. Acta 1568 (2001) 237–244, https://doi.org/10.1016/s0304-4165(01)00226-4.

[39] J.R. Gionfriddo, K.S. Freeman, A. Groth, V.L. Scofield, K. Alyahya, J.E. Madl, alpha-Luminol prevents decreases in glutamate, glutathione, and glutamine synthetase in the retinas of glaucomatous DBA/2J mice, Vet. Ophthalmol. 12 (2009) 325–332, https://doi.org/10.1111/j.1463-5224.2009.00722.x.
[40] X. Zhang, Z. Feng, C. Li, Y. Zheng, Morphological and migratory alterations in retinal Muller cells during early stages of hypoxia and oxidative stress, AIMS Mol. Sci. 7 (2012) 31–35, https://doi.org/10.3969/j.issn.1673-5374.2012.01.005.
[41] Q. Liu, F. Zhang, X. Zhang, R. Cheng, J.X. Ma, J. Yi, et al., Fenofibrate ameliorates diabetic retinopathy by modulating Nrf2 signaling and NLRP3 inflammasome activation, Mol. Cell. Biochem. 445 (2018) 105–115, https://doi.org/10.1007/s11010-017-3256-x.
[42] J.M. Kim, S.H. Cha, Y.R. Choi, I. Jou, E.H. Joe, S.M. Park, DJ-1 deficiency impairs glutamate uptake into astrocytes via the regulation of flotillin-1 and caveolin-1 expression, Sci. Rep. 6 (2016) 28823, https://doi.org/10.1038/srep28823.
[43] H. Nishinaga, K. Takahashi-Niki, T. Taira, A. Andreadis, S.M. Iguchi-Ariga, H. Ariga, Expression profiles of genes in DJ-1-knockdown and L 166 P DJ-1 mutant cells, Neurosci. Lett. 390 (2005) 54–59, https://doi.org/10.1016/j.neulet.2005.07.053.
[44] S. Yamaguchi, T. Yamane, K. Takahashi-Niki, I. Kato, T. Niki, M.S. Goldberg, et al., Transcriptional activation of low-density lipoprotein receptor gene by DJ-1 and effect of DJ-1 on cholesterol homeostasis, PloS One 7 (2012), e38144, https://doi.org/10.1371/journal.pone.0038144.
[45] J.W. Baynes, The role of AGEs in aging: causation or correlation, Exp. Gerontol. 36 (2001) 1527–1537, https://doi.org/10.1016/s0531-5565(01)00138-3.
[46] V.L. Bonilha, Age and disease-related structural changes in the retinal pigment epithelium, Clin. Ophthalmol. 2 (2008) 413–424, https://doi.org/10.2147/opth.s2151.
[47] S. Yoshida, B.M. Yashar, S. Hiriyanna, A. Swaroop, Microarray analysis of gene expression in the aging human retina, Invest. Ophthalmol. Vis. Sci. 43 (2002) 2554–2560.
[48] H. Ida, S.A. Boylan, A.L. Weigel, L.M. Hjelmeland, Age-related changes in the transcriptional profile of mouse RPE/choroid, Physiol. Genom. 15 (2003) 258–262, https://doi.org/10.1152/physiolgenomics.00126.200300126.2003.
[49] M.M. Sachdeva, M. Cano, J.T. Handa, Nrf2 signaling is impaired in the aging RPE given an oxidative insult, Exp. Eye Res. 119 (2014) 111–114, https://doi.org/10.1016/j.exer.2013.10.024.
[50] J. Du, A. Yanagida, K. Knight, A.L. Engel, A.H. Vo, C. Jankowski, et al., Reductive carboxylation is a major metabolic pathway in the retinal pigment epithelium, Proc. Natl. Acad. Sci. U. S. A. 113 (2016) 14710–14715, https://doi.org/10.1073/pnas.1604572113.
[51] M.A. Kanow, M.M. Giarmarco, C.S. Jankowski, K. Tsantilas, A.L. Engel, J. Du, et al., Biochemical adaptations of the retina and retinal pigment epithelium support a metabolic ecosystem in the vertebrate eye, Elife 6 (2017), https://doi.org/10.7554/eLife.28899.
[52] C.M. Clements, R.S. McNally, B.J. Conti, T.W. Mak, J.P. Ting, DJ-1, a cancer- and Parkinson's disease-associated protein, stabilizes the antioxidant transcriptional master regulator Nrf2, Proc. Natl. Acad. Sci. U. S. A. 103 (2006) 15091–15096, https://doi.org/10.1073/pnas.0607260103.
[53] L. Gan, D.A. Johnson, J.A. Johnson, Keap1-Nrf2 activation in the presence and absence of DJ-1, Eur. J. Neurosci. 31 (2010) 967–977, https://doi.org/10.1111/j.1460-9568.2010.07138.x.
[54] Y.F. Yan, H.P. Chen, X.S. Huang, L.Y. Qiu, Z.P. Liao, Q.R. Huang, DJ-1 mediates the delayed cardioprotection of hypoxic preconditioning through activation of Nrf2 and subsequent upregulation of antioxidative enzymes, J. Cardiovasc. Pharmacol. 66 (2015) 148–158, https://doi.org/10.1097/FJC.0000000000000257.
[55] P. Lopert, M. Patel, Brain mitochondria from DJ-1 knockout mice show increased respiration-dependent hydrogen peroxide consumption, Redox Biol. 2 (2014) 667–672, https://doi.org/10.1016/j.redox.2014.04.010.
[56] E. Andres-Mateos, C. Perier, L. Zhang, B. Blanchard-Fillion, T.M. Greco, B. Thomas, et al., DJ-1 gene deletion reveals that DJ-1 is an atypical peroxiredoxin-like peroxidase, Proc. Natl. Acad. Sci. U. S. A. 104 (2007) 14807–14812, https://doi.org/10.1073/pnas.0703219104.
[57] S.V. Petersen, T.D. Oury, Z. Valnickova, I.B. Thogersen, P. Hojrup, J.D. Crapo, et al., The dual nature of human extracellular superoxide dismutase: one sequence and two structures, Proc. Natl. Acad. Sci. U. S. A. 100 (2003) 13875–13880, https://doi.org/10.1073/pnas.2436143100.
[58] N. Fujiwara, M. Nakano, S. Kato, D. Yoshihara, T. Ookawara, H. Eguchi, et al., Oxidative modification to cysteine sulfonic acid of Cys111 in human copper-zinc superoxide dismutase, J. Biol. Chem. 282 (2007) 35933–35944, https://doi.org/10.1074/jbc.M702941200.